1 **Revision 2**

# 2 The iron spin transition of deep nitrogen-bearing mineral $Fe_3N_{1.2}$ at 3 high pressure

4

5 Chaojia Lv[1], Jin Liu[1,2]

6 [1]*Center for High Pressure Science and Technology Advanced Research, Beijing 100094, China*

7 [2]*CAS Center for Excellence in Deep Earth Science, Guangzhou 510640, China*

8 *Correspondence to: J. Liu (jin.liu@hpstar.ac.cn)

9

## 10 Highlights:

11 1) *In-situ* X-ray emission spectroscopy measurements were performed on $Fe_3N_{1.2}$ up to 45.8
12 GPa at room temperature.

13 2) The pressure-induced spin transition of iron in $Fe_3N_{1.2}$ starts at relatively low pressures and
14 completes at ~ 30.5 GPa.

15 3) The iron spin transition pressure is highly related to the nitrogen concentration of
16 hexagonal iron nitrides.

17 4) The identity and concentration of light elements, together with crystal structure, may take
18 charge of the spin transition pressure of iron-rich alloys.

19

This is the peer-reviewed, final accepted version for American Mineralogist, published by the Mineralogical Society of America.
The published version is subject to change. Cite as Authors (Year) Title. American Mineralogist, in press.
DOI: https://doi.org/10.2138/am-2022-8434. http://www.minsocam.org/

## Abstract

Nitrogen is an essential element for life, one of the most abundant volatiles in the atmosphere, and an important component in the Earth's interior, where iron nitride is an essential host of deep nitrogen. Here, we investigate the pressure-induced electronic spin-pairing transition of iron in siderazot ($Fe_3N_{1.2}$) at pressures to 45.8 GPa at room temperature, using diamond-anvil cell techniques coupled with synchrotron x-ray emission spectroscopy. The integrated intensity of the satellite emission peak ($K_\beta'$) decreases once upon compression and remains unchanged at pressures greater than 30.5 GPa. In other words, the high-spin to low-spin transition of iron in $Fe_3N_{1.2}$ starts immediately at very low pressures and completes at ~ 30.5 GPa. The iron spin transition completion pressures increase with the nitrogen concentration of hexagonal close-packed iron nitrides (i.e., $Fe_3N_{1.2}$, $Fe_7N_3$, and $Fe_2N$). Moreover, the identity and concentration of light elements, together with their crystal structure, could affect the iron spin transition pressure of binary iron-rich compounds such as $Fe_3N$, $Fe_3C$, $Fe_3P$, $Fe_3S$, $Fe_7C_3$, and $Fe_7N_3$. The spin transition of iron-rich alloys could alter the bonding nature and the physical properties including the thermal and electrical conductivity, influencing the thermal state and evolution of planetary interiors in turn.

**Keywords:** spin transition, x-ray emission spectroscopy, high pressure, deep nitrogen

## Introduction

Nitrogen is a key probe to understand the accretion and degassing of volatiles and the differentiation and evolution history of the Earth. It is also one of the most poorly studied elements under the Earth's deep interior pressure and temperature (*P*-*T*) conditions. Surface and deep nitrogen are largely connected via subduction and volcanic degassing [*Halama et al.*, 2012; *Mao and Mao*, 2020; *Halama and Bebout*, 2021]. Notably, the nitrogen concentration in the present-day bulk silicate Earth may be only tens of ppm, severely depleted with respect to other volatiles like carbon and sulfur [*Marty*, 2012; *Bergin et al.*, 2015; *Yoshioka et al.*, 2018]. Apart from volatile degassing during accretion, the metallic core has been considered a hidden reservoir to account for the missing nitrogen according to the siderophile nature of nitrogen as revealed in metal-silicate partition experiments [*Hirschmann*, 2016; *Li et al.*, 2016; *Dalou et al.*, 2017; *Dalou et al.*, 2019]. Up to 0.5 wt.% nitrogen, together with other candidate light elements of Si, O, C, S, and H, has been suggested in the Earth's core to interpret the core density deficit based on the global seismic models, e.g., the Preliminary Reference Earth Model (PREM) [*Dziewonski and Anderson*, 1981; *Sugiura*, 1998]. In addition, the deep mantle becomes relatively reduced with the ~ 1 wt% metallic iron that is saturated at depths greater than 250 km [*Rohrbach et al.*, 2007]. Based on the presence of iron nitrides and carbonitrides in meteorites and deep diamond inclusions, nitrogen may be distributed heterogeneously and enriched in metal phases in the Earth's interior [*Li and Keppler*, 2014; *Litasov et al.*, 2017; *Rubin and Ma*, 2017; *Huang et al.*, 2021].

Iron nitrides have been widely suggested as the primary hosts of deep nitrogen in the reduced Earth's interior; their thermostability and phase relations have attracted extensive attention. Among these Fe-N intermediates, orthorhombic ζ-$Fe_2N$ (space group: *Pbcn*), cubic γ′-$Fe_4N$ (space group: $Pm\bar{3}m$), and nonstoichiometric siderazot ε-$Fe_3N_x$ ($0.75<x<1.5$) are stable at ambient conditions [*Niellsen and Burhwald*, 1981; *Minobe et al.*, 2015; *Litasov et al.*, 2017; *Yoshioka et al.*, 2018]. Under compression, ε-$Fe_3N_x$ forms from $Fe_2N$ and $Fe_4N$ at 9-15 GPa and 1400-1600 K [*Schwarz et al.*, 2009; *Guo et al.*, 2013]. It has either a $P3_12$ or $P6_322$ space group with hexagonal close-packed iron atoms while nitrogen atoms occupy part of the octahedral voids [*Sifkovits et al.*, 1999; *Guo et al.*, 2013; *Bette et al.*, 2021]. The ε-$Fe_3N_x$ phase is the same as the ε-$Fe_7N_3$ phase when $x$ is equal to ~ 1.3. $Fe_7N_3$ undergoes the pressure-induced phase transition from ε to β crystal structures at pressures greater than 41 GPa and ~ 1000 K while the β-$Fe_7N_3$ has been considered a candidate nitrogen-bearing phase in the Earth's core [*Minobe et al.*, 2015; *Kusakabe et al.*, 2019]. Additionally, previous studies reported that the ε-$Fe_3N_x$ phase is stable at least up to 60 GPa at room temperature [*Lv et al.*, 2020; *Huang et al.*, 2021]. To date, the effects of nitrogen concentration on the stability and physical properties of nonstoichiometric ε-$Fe_3N_x$ have not been investigated.

The iron 3*d* orbitals collapse under extremely high pressures of the deep Earth, leading to the high-spin to low-spin transition of iron-bearing minerals. The configuration and interaction of the outermost shell electrons of iron, which are dramatically altered by pressure, are essentially significant for materials' physical and chemical properties [*Liu et al.*, 2019; *Zhao et al.*, 2020]. The pressure-induced spin transition of iron greatly changes the chemical

bonding of relevant minerals and thus, affects thermodynamic properties, rheology, and the thermal and electrical conductivity of iron-bearing minerals [*Lin et al.*, 2013]. The iron spin transition occurs widely in the deep mantle for both iron-bearing oxide-hydroxides and metallic compounds [*Lin et al.*, 2004a; *Lin and Tsuchiya*, 2008; *Gu et al.*, 2014; *Chen et al.*, 2018; *Su et al.*, 2021]. At ambient conditions, the 3*d*-orbit electrons of Fe in all iron nitrides are in a high-spin ferromagnetic arrangement [*Sifkovits et al.*, 1999]. The magnetic moment of Fe-N compounds generally decreases with increasing nitrogen concentration, and it is about 2.0 $\mu_B$ for ε-$Fe_3N$ [*Panda and Gajbhiye*, 1997; *Leineweber et al.*, 2001; *Guo et al.*, 2013]. The iron spin transition has been widely reported for the Fe-C, Fe-S, and Fe-P systems, while it has only been investigated in the Fe-N system for γ′-$Fe_4N$ and ε-$Fe_7N_3$ under high pressure [*Ishimatsu et al.*, 2003; *Lv et al.*, 2020]. *Lv et al.* [2020] revealed that the iron spin transition of ε-$Fe_7N_3$ completes at 43 GPa and 300 K, but it may not apply to other ε-$Fe_3N_x$ compositions. Thus far, the effects of nitrogen on the iron spin transition pressure remains poorly constrained with respect to other light elements because the crystal structure and arrangement of iron 3*d*-orbital electrons could be affected by nitrogen concentration [*Widenmeyer et al.*, 2014].

In this work, the spin transition of iron in ε-$Fe_3N_{1.2}$ is determined in diamond-anvil cells by synchrotron x-ray emission spectroscopy (XES) at high pressure. First, the magnetic spin state of iron in ε-$Fe_3N_{1.2}$ is measured up to 45.8 GPa at 300 K. The high-spin to low-spin transition of iron in ε-$Fe_3N_{1.2}$ starts at pressures below 9.8 GPa and completes at ~ 30.5 GPa. Then, we evaluate the effects of nitrogen concentration on iron nitrides' spin transition

100 pressure by comparing with previous studies on the spin transition of iron-rich alloys.
101 Furthermore, it is discussed how the identity and concentration of light elements regulate the
102 iron spin transition pressure of candidate iron-rich alloys.
103

104 ## Methods

105 The $\varepsilon$-$Fe_3N_x$ polycrystalline (Lot#: RA191101) sample was obtained from Antechnology
106 Co., Ltd, Beijing. Previous studies suggested the ideal space group for ε-$Fe_3N_x$ is either $P3_12$
107 or $P6_322$ and their structural differences are subtle and challenging to be recognized by x-ray
108 diffraction measurements [*Guo et al.*, 2013]. Moreover, the $P3_12$ space group has been
109 recommended for nonstoichiometric ε-$Fe_3N_x$ while $P6_322$ for stoichiometric ε-$Fe_7N_3$
110 [*Leineweber et al.*, 2001; *Niewa et al.*, 2009; *Lv et al.*, 2020]. In this work, the x-ray
111 diffraction pattern of ε-$Fe_3N_x$ at ambient conditions confirms its hexagonal crystal structure in
112 the space group of $P3_12$ and unit cell volume of 85.788(75) $Å^3$ with unit cell parameters
113 $a$=$b$=4.740(1) Å and $c$=4.409(2) Å. On the basis of the empirical relationship between the
114 unit cell volume and nitrogen content of iron nitrides [*Litasov et al.*, 2017], the
115 polycrystalline sample has a mildly higher nitrogen content than stoichiometric ε-$Fe_3N$ with
116 the chemical formula of $Fe_3N_{1.216(7)}$. For simplification, $Fe_3N_{1.2}$ is used to represent the
117 ε-$Fe_3N_{1.216(7)}$ sample hereafter in this study.
118 The $Fe_3N_{1.2}$ sample of ~ 60 μm in diameter and ~ 8 μm thick was loaded into a diamond
119 anvil cell with a flat culet size of 300 μm. The Be gasket was pre-indented to 20–25 μm thick,
120 and a hole of 200 um in diameter was drilled into the center of the indentation. Cubic boron

121 nitride (cBN)-epoxy powder was packed into this hole and then compacted to 20 GPa at room
122 temperature. A hole of ~ 100 μm in diameter was finally drilled into the center of the cBN
123 gasket insert to serve as the sample chamber using the laser drilling system at the Center for
124 High Pressure Science and Technology Advanced Research (HPSTAR), Beijing. Silicone oil
125 was used as a pressure-transmitting medium and two 5–8 μm-sized ruby spheres were placed
126 next to the sample as pressure calibration [*Mao et al.*, 1986]. The pressure was measured and
127 averaged over multiple times before and after XES measurements at a given pressure, and its
128 uncertainty is mostly less than 3%.

129 High-pressure x-ray emission spectra of $Fe_3N_{1.2}$ were collected between 2.9 and 45.8
130 GPa at room temperature at the HPCAT beamline 16-ID-D of the Advanced Photon Source,
131 Argonne National Laboratory. The incident x-ray beam of 11.3 keV with the full width at half
132 maximum (FWHM) of less than 1 eV was focused down to ~ 20 μm vertically and
133 horizontally at the sample position. The Fe emission signal was collected from 7020 to 7080
134 eV with an energy step of 0.3 eV using a Peltier-cooled silicon detector after being selected
135 by a silicon analyzer [*Liu et al.*, 2019]. Helium gas was filled into the x-ray path to reduce the
136 absorption by air. Each XES spectrum was collected for ~ 1 hour, and three XES spectra were
137 accumulated at each pressure. All spectra were normalized to the transmitted intensity, and
138 the $K_\beta$ main peaks were aligned to 7058 eV [*Liu et al.*, 2019]. The intensity difference of the
139 satellite peak $K_\beta'$ was integrated from 7030 to 7053 eV using the integrated relative difference
140 (IRD) method [*Chen et al.*, 2014]. Compared with the integrated absolute difference (IAD)
141 method, the IRD method aligns the main peaks to the same energy position, which could

This is the peer-reviewed, final accepted version for American Mineralogist, published by the Mineralogical Society of America.
The published version is subject to change. Cite as Authors (Year) Title. American Mineralogist, in press.
DOI: https://doi.org/10.2138/am-2022-8434. http://www.minsocam.org/

avoid the broadening effect of the $K_{\beta 1,3}$ peak in modelling the spin momentum reduction with increasing pressure [*Mao et al.*, 2014; *Lin et al.*, 2016].

## Results and Discussion

The magnetic order and spin state of iron in $Fe_3N_{1.2}$ were probed by the $K_\beta$ fluorescence peaks from the XES spectra up to 45.8 GPa (Figure 1). Each $K_\beta$ emission spectrum at a given pressure can be divided into a main $K_{\beta 1,3}$ peak and a lower-energy satellite $K_\beta'$ peak due to the final state interaction between the 3*p* core hole and the electrons of the partially filled 3*d* shell of iron [*Gu et al.*, 2016; *Liu et al.*, 2019]. All spectra were normalized to the transmitted intensity and then shifted to set the $K_{\beta 1,3}$ emission lines to 7058 eV. The intensity of the $K_\beta'$ peak is indicative of the spin state and total spin moment of iron in $Fe_3N_{1.2}$. As the pressure increases, a gradual reduction of the $K_\beta'$ peak corresponds to the pressure-induced high-spin to low-spin transition of iron [*Lin et al.*, 2005]. The integrated intensity of the $K_\beta'$ peak is plotted between 7030 and 7053 eV and fitted to the Boltzmann function in Figure 2. Upon compression, the intensity of the satellite $K_\beta'$ peak decreases gradually up to 30.5 GPa and remains unchanged at higher pressures. The steep slope in the relationship between the high-spin fraction and pressure under relatively low pressures indicates that the spin transition of iron in $Fe_3N$ starts at pressure below 2.9−9.8 GPa. Moreover, the unchanged intensity of the $K_\beta'$ peak at pressures over 30.5 GPa suggests the completion of the iron spin transition of $Fe_3N_{1.2}$ at ~ 30.5 GPa.

The magnetic state is highly related to the spin transition of iron in $Fe_3N_{1.2}$. At ambient conditions, $Fe_3N_{1.2}$ is in a ferromagnetic (FM) state while all the 3*d* orbitals of Fe are occupied with four unpaired electrons [*Leineweber et al.*, 2001; *Lin et al.*, 2013]. The high-spin to low-spin transition of $Fe_3N_{1.2}$ completes at ~ 30.5 GPa, likely corresponding to the FM to nonmagnetic (NM) transition. We note that the FM to paramagnetic (PM) transition cannot be detected with the XES measurements due to the relative orientations of individual spins [*Lv et al.*, 2020]. The compression behavior may provide an indirect measurement for the FM-PM transition in the Fe-N system, which has been observed in other Fe-light element compounds like $Fe_7C_3$ [*Chen et al.*, 2014]. Among the Fe-N compounds, the discontinuity of the unit cell volume of $Fe_4N$ at ~ 24 GPa in *Zhuang et al.* [2021] may correspond to the FM-PM transition, as suggested by *Ishimatsu et al.* [2003] using XMCD measurements. However, this method might not be applicable for ε-$Fe_3N_x$ because of its relatively smooth compression behavior [*Adler and Williams*, 2005; *Lv et al.*, 2020]. It should be noted that the plateau in the relationship between the unit cell volume and pressure in *Adler and Williams* [2005] is likely caused by the nonhydrostatic conditions. Previous ab initio calculations predicted the spin transition of iron in ε-$Fe_3N$ at ~ 125 GPa and 0 K, which is inconsistent with our XES results [*Popov et al.*, 2015]. Nevertheless, further work is needed to decode the FM-PM transition in the ε-$Fe_3N_x$ by using XMCD or Mössbauer spectroscopy measurements.

The nitrogen concentration, together with the crystal structure, may control the magnetism properties of iron nitrides such as ζ-$Fe_2N$, ε-$Fe_3N$, ε-$Fe_7N_3$, and γ′-$Fe_4N$. In the

183 lattices of these Fe-N compounds, nitrogen atoms occupy the octahedral sites with strong
184 covalent *p-d* bonds, which greatly influences the magnetic moments [*Sifkovits et al.*, 1999;
185 *Guo et al.*, 2013]. At ambient conditions, the γ′-$Fe_4N$ is based on the face-centered cubic
186 structure of iron with 1/4 of the octahedral voids occupied by nitrogen, carrying a moment of
187 about 2.0 $\mu_B$. Moreover, ζ-$Fe_2N$, ε-$Fe_7N_3$, and ε-$Fe_3N$ are based on the (slightly distorted)
188 hexagonal close-packed lattice of iron with 1/2, 3/7, and 1/3 of the octahedral voids occupied
189 by nitrogen, respectively [*Sifkovits et al.*, 1999]. The number of nearest neighboring nitrogen
190 atoms for each iron atom varies from 2 to 3, resulting in a magnetic moment reduction from
191 2.0 to 1.5 $\mu_B$ for these hexagonal iron nitrides [*Panda and Gajbhiye*, 1997]. In other words,
192 the nitrogen concentration could strongly influence the nature of the pressure-induced spin
193 transition of iron nitrides.

194 The completion pressures of the iron spin transition for all the iron nitrides are higher
195 than pure iron. As shown in Figure 2, the spin transition completion pressures for metallic
196 iron is ~ 13 GPa, which corresponds to the bcc-hcp phase transition at 300 K [*Monza et al.*,
197 2011]. This suggests a positive effect of nitrogen on the spin transition completion pressure.
198 The spin transition completion pressure of $Fe_3N_{1.2}$ in this work is lower than that of $Fe_7N_3$
199 reported by *Lv et al.* [2020], though the experimental settings are nearly identical. The
200 different completion pressures indicate that nitrogen concentration mostly dictates the iron
201 spin transition of the hexagonal Fe-N compounds. In addition, this trend is further confirmed
202 because $Fe_2N$ with higher nitrogen concentration shows a higher spin transition completion
203 pressure. These results suggest that more nitrogen in the Fe-N hexagonal lattice provides

more covalent bonds, which likely enhances the structural stability against compression [*Sifkovits et al.*, 1999]. On the other hand, γ′-$Fe_4N$ shows a relatively high spin transition completion pressure while its nitrogen content is much lower than ε-$Fe_3N$. This may be attributed to the difference in the crystal structure and nature of Fe-N bonding. There are two different Fe sites in γ′-$Fe_4N$: Fe(I) is similar to fcc-Fe, and Fe(II) has two nearest neighboring nitrogen atoms, whereas all the Fe atoms are equally sited in hexagonal iron nitrides like ε-$Fe_3N$ [*Sifkovits et al.*, 1999]. Therefore, nitrogen concentrations, together with crystal structures, primarily control the iron spin transition of iron nitrides at high pressure. The completion pressures of spin transition of iron in $Fe_3C$ and $Fe_7C_3$ also exhibit a similar trend on how carbon concentration affects the pressure range of the iron spin transition in the Fe-C system [*Chen et al.*, 2018].

## Implications

The iron spin transition has been widely observed in iron-rich Fe-light element alloys, such as the Fe-C, Fe-N, Fe-S, and Fe-P systems [*Ishimatsu et al.*, 2003; *Lin et al.*, 2004a; *Lin et al.*, 2004b; *Chen et al.*, 2014; *Gu et al.*, 2014; *Gu et al.*, 2016; *Chen et al.*, 2018; *Lai et al.*, 2020; *Lv et al.*, 2020]. The spin transitions of iron in these Fe-light element alloys are often associated with a volume collapse. Consequently, the equation of state for the low-spin state differs from that for the high-spin state at given *P-T* conditions [*Chen et al.*, 2014; *Lai et al.*, 2020; *Lv et al.*, 2020]. The spin transition pressures of various Fe-rich binary alloys are compared in Figure 3. The spin transition completion pressures of iron in the two iron

carbides are greater than in iron nitrides, suggesting carbon has a stronger lattice stabilizing effect than nitrogen. The large difference in the spin transition completion pressures between $Fe_3N_{1.2}$ and $Fe_3C$ may result from different crystal structures. On the contrary, the spin transition pressures are comparable between $Fe_7N_3$ and $Fe_7C_3$. We note that $Fe_7N_3$, $Fe_7C_3$, and $Fe_3N_{1.2}$ have a hexagonal lattice, while $Fe_3C$ has an orthorhombic structure [*Caracas*, 2016]. Moreover, the spin transition completion pressures of iron sulfide $Fe_3S$ and iron phosphide $Fe_3P$ are relatively lower than iron carbides and nitrides. Such pressure differences could be ascribed to the tetragonal crystal structure of $Fe_3S$ and $Fe_3P$ because both sulfur and phosphorus have larger atomic radii [*Slater*, 1964]. Similarly, the spin transition onset pressures are also different from each other. The iron spin transition of $Fe_3N$ starts at pressures lower than 5-10 GPa, whereas other iron nitrides and all iron carbides undergo the electronic spin-pairing transition of iron at pressures greater than 10 GPa. Notably, the iron spin transition of all the iron-rich phosphides and sulfides starts at very low pressures under compression. Therefore, the identity and concentration of light elements in the metallic cores of terrestrial planets and asteroids may control the spin state of iron at high pressure.

The spin transition completion pressure may be positively correlated with high temperatures for iron alloyed with light elements. Previous studies found that the mixed spin state of iron widens with increasing temperature in ferropericlase, iron-bearing carbonate, and metallic iron [*Tsuchiya et al.*, 2006; *Lin et al.*, 2007; *Liu et al.*, 2014; *Ono*, 2015]. In addition, the onset pressure of the iron spin transition could be slightly increased with increasing temperature, while the completion pressure may be enhanced significantly with increasing

temperature. The HS-LS boundary slope varies among previous studies, and it is about 0.045 K/GPa for hcp-Fe [*Ono*, 2015]. Assuming that iron-rich alloys share a similar slope as pure iron under high temperatures, all the Fe-C, Fe-N, Fe-S, and Fe-P systems might be in LS state in the mantle and core of the present-day Earth [*Katsura et al.*, 2010]. On the other hand, the spin crossover of iron-rich alloys may occur under the *P-T* conditions of small terrestrial planets, e.g., Mars and Mercury [*Smith et al.*, 2012; *Margot et al.*, 2018; *Stähler et al.*, 2021]. Furthermore, the spin transition of iron in $Fe_3N$ and other iron-rich alloys could have an influence on the compressibility and conductivity of solid metallic cores of terrestrial planets, likely controlling the nucleation pattern, thermal dynamo, and structure of planetary interiors.

**Acknowledgments**

We thank Yuming Xiao, Paul Chow, and Xiaowan Su for their experimental assistance. This work is supported by the National Natural Science Foundation of China (NSFC grant 42072052). Synchrotron XES measurements were performed at the High-Pressure Collaborative Access Team (HPCAT 16-IDD), APS, ANL. HPCAT operations are supported by DOE-NNSA's Office of Experimental Sciences. The Advanced Photon Source is a U.S. Department of Energy (DOE) Office of Science User Facility operated for the DOE Office of Science by Argonne National Laboratory under Contract No. DE-AC02-06CH11357. Some experiments are supported by the Synergic Extreme Condition User Facility (SECUF).

## References

Adler, J. F., and Williams, Q. (2005), A high-pressure X-ray diffraction study of iron nitrides: Implications for Earth's core, *Journal of Geophysical Research*, *110*(B1), B01203, doi:10.1029/2004jb003103.

Bergin, E. A., Blake, G. A., Ciesla, F., Hirschmann, M. M., and Li, J. (2015), Tracing the ingredients for a habitable earth from interstellar space through planet formation, *Proceedings of the National Academy of Sciences*, *112*(29), 8965-8970, doi:10.1073/pnas.1500954112.

Bette, S., Theye, T., Bernhardt, H.-J., Clark, W. P., and Niewa, R. (2021), Confirmation of siderazot, $Fe_3N_{1.33}$, the only terrestrial nitride mineral, *Minerals*, *11*(3), 290, doi:10.3390/min11030290.

Caracas, R. (2016), Crystal structures of core materials, in *Deep Earth: Physics and Chemistry of the Lower Mantle and Core*, edited by Terasaki, H. and Fischer, R. A., pp. 55-68, Wiley, doi:10.1002/9781118992487.ch5.

Chen, B., Lai, X., Li, J., Liu, J., Zhao, J., Bi, W., et al. (2018), Experimental constraints on the sound velocities of cementite $Fe_3C$ to core pressures, *Earth and Planetary Science Letters*, *494*, 164-171, doi:10.1016/j.epsl.2018.05.002.

Chen, B., Li, Z., Zhang, D., Liu, J., Hu, Y. M., Zhao, J., et al. (2014), Hidden carbon in Earth's inner core revealed by shear softening in dense $Fe_7C_3$, *Proceedings of the National Academy of Sciences*, *111*(50), 17755-17758, doi:10.1073/pnas.1411154111.

Dalou, C., Furi, E., Deligny, C., Piani, L., Caumon, M.-C., Laumonier, M., et al. (2019), Redox control on nitrogen isotope fractionation during planetary core formation, *Proceedings of the National Academy of Sciences*, *116*(29), 14485-14494, doi:10.1073/pnas.1820719116.

Dalou, C., Hirschmann, M. M., von der Handt, A., Mosenfelder, J., and Armstrong, L. S. (2017), Nitrogen and carbon fractionation during core-mantle differentiation at shallow depth, *Earth and Planetary Science Letters*, *458*, 141-151, doi:10.1016/j.epsl.2016.10.026.

Dziewonski, A. M., and Anderson, D. L. (1981), Preliminary reference Earth model, *Physics of the Earth and Planetary Interiors*, *25*(4), 297-356, doi:10.1016/0031-9201(81)90046-7.

Gu, T., Fei, Y., Wu, X., and Qin, S. (2014), High-pressure behavior of $Fe_3P$ and the role of phosphorus in planetary cores, *Earth and Planetary Science Letters*, *390*, 296-303, doi:10.1016/j.epsl.2014.01.019.

Gu, T., Fei, Y., Wu, X., and Qin, S. (2016), Phase stabilities and spin transitions of $Fe_3(S_{1-x}P_x)$ at high pressure and its implications in meteorites, *American Mineralogist*, *101*(1), 205-210, doi:10.2138/am-2016-5466.

Guo, K., Rau, D., von Appen, J., Prots, Y., Schnelle, W., Dronskowski, R., et al. (2013), High pressure high-temperature behavior and magnetic properties of $Fe_4N$: Experiment and theory, *High Pressure Research*, *33*(3), 684-696, doi:10.1080/08957959.2013.809715.

Halama, R., and Bebout, G. (2021), Earth's nitrogen and carbon cycles, *Space Science Reviews*, *217*(3), 45, doi:10.1007/s11214-021-00826-7.

Halama, R., Bebout, G. E., John, T., and Scambelluri, M. (2012), Nitrogen recycling in subducted mantle rocks and implications for the global nitrogen cycle, *International Journal of Earth Sciences*, *103*(7), 2081-2099, doi:10.1007/s00531-012-0782-3.

Hirschmann, M. M. (2016), Constraints on the early delivery and fractionation of Earth's major volatiles from C/H, C/N, and C/S ratios, *American Mineralogist*, *101*(3), 540-553, doi:10.2138/am-2016-5452.

306 Huang, S., Wu, X., Zhu, F., Lai, X., Li, J., Neill, O. K., et al. (2021), High-pressure phase stability and
307 thermoelastic properties of iron carbonitrides and nitrogen in the deep Earth, *Journal of Geophysical*
308 *Research: Solid Earth*, *126*(6), B021934, doi:10.1029/2021jb021934.
309 Ishimatsu, N., Maruyama, H., Kawamura, N., Suzuki, M., Ohishi, Y., Ito, M., et al. (2003), Pressure-induced
310 magnetic transition in $Fe_4N$ probed by Fe *K*-edge XMCD measurement, *Journal of the Physical Society of*
311 *Japan*, *72*(9), 2372-2376, doi:10.1143/jpsj.72.2372.
312 Katsura, T., Yoneda, A., Yamazaki, D., Yoshino, T., and Ito, E. (2010), Adiabatic temperature profile in the
313 mantle, *Physics of the Earth and Planetary Interiors*, *183*(1-2), 212-218, doi:10.1016/j.pepi.2010.07.001.
314 Kusakabe, M., Hirose, K., Sinmyo, R., Kuwayama, Y., Ohishi, Y., and Helffrich, G. (2019), Melting curve and
315 equation of state of β-$Fe_7N_3$: Nitrogen in the Core?, *Journal of Geophysical Research: Solid Earth*, *124*(4),
316 3448-3457, doi:10.1029/2018jb015823.
317 Lai, X., Zhu, F., Liu, Y., Bi, W., Zhao, J., Alp, E. E., et al. (2020), Elastic and magnetic properties of $Fe_3P$ up to
318 core pressures: Phosphorus in the Earth's core, *Earth and Planetary Science Letters*, *531*(1), 115974,
319 doi:10.1016/j.epsl.2019.115974.
320 Leineweber, A., Jacobs, H., Hüning, F., Lueken, H., and Kockelmann, W. (2001), Nitrogen ordering and
321 ferromagnetic properties of ϵ-$Fe_3N_{1+x}$ ($0.10 \leq x \leq 0.39$) and ϵ-$Fe_3(N_{0.80}C_{0.20})_{1.38}$, *Journal of Alloys and*
322 *Compounds*, *316*(1-2), 21-38, doi:10.1016/s0925-8388(00)01435-3.
323 Li, Y., and Keppler, H. (2014), Nitrogen speciation in mantle and crustal fluids, *Geochimica et Cosmochimica*
324 *Acta*, *129*, 13-32, doi:10.1016/j.gca.2013.12.031.
325 Li, Y., Marty, B., Shcheka, S., Zimmermann, L., and Keppler, H. (2016), Nitrogen isotope fractionation during
326 terrestrial core-mantle separation, *Geochemical Perspectives Letters*, *2*, 138-147,
327 doi:10.7185/geochemlet.1614.
328 Lin, J.-F., Fei, Y., Sturhahn, W., Zhao, J., Mao, H.-k., and Hemley, R. J. (2004a), Magnetic transition and sound
329 velocities of $Fe_3S$ at high pressure: Implications for Earth and planetary cores, *Earth and Planetary Science*
330 *Letters*, *226*(1-2), 33-40, doi:10.1016/j.epsl.2004.07.018.
331 Lin, J.-F., Speziale, S., Mao, Z., and Marquardt, H. (2013), Effects of the electronic spin transitions of iron in
332 lower mantle minerals: Implications for deep mantle geophysics and geochemistry, *Reviews of Geophysics*,
333 *51*(2), 244-275, doi:10.1002/rog.20010.
334 Lin, J.-F., Struzhkin, V. V., Mao, H.-k., Hemley, R. J., Chow, P., Hu, M. Y., et al. (2004b), Magnetic transition in
335 compressed $Fe_3C$ from X-ray emission spectroscopy, *Physical Review B*, *70*(21), 212405,
336 doi:10.1103/PhysRevB.70.212405.
337 Lin, J.-F., and Tsuchiya, T. (2008), Spin transition of iron in the Earth's lower mantle, *Physics of the Earth and*
338 *Planetary Interiors*, *170*(3-4), 248-259, doi:10.1016/j.pepi.2008.01.005.
339 Lin, J. F., Mao, Z., Yang, J., Liu, J., Xiao, Y., Chow, P., et al. (2016), High-spin $Fe^{2+}$ and $Fe^{3+}$ in single-crystal
340 aluminous bridgmanite in the lower mantle, *Geophysical Research Letters*, *43*(13), 6952-6959,
341 doi:10.1002/2016gl069836.
342 Lin, J. F., Struzhkin, V. V., Jacobsen, S. D., Hu, M. Y., Chow, P., Kung, J., et al. (2005), Spin transition of iron in
343 magnesiowustite in the Earth's lower mantle, *Nature*, *436*(7049), 377-380, doi:10.1038/nature03825.
344 Lin, J. F., Vanko, G., Jacobsen, S. D., Iota, V., Struzhkin, V. V., Prakapenka, V. B., et al. (2007), Spin transition
345 zone in Earth's lower mantle, *Science*, *317*(5845), 1740-1743, doi:10.1126/science.1144997.

Litasov, K. D., Shatskiy, A., Ponomarev, D. S., and Gavryushkin, P. N. (2017), Equations of state of iron nitrides ε-$Fe_3N_x$ and γ-$Fe_4N_y$ to 30 GPa and 1200 K and implication for nitrogen in the Earth's core, *Journal of Geophysical Research: Solid Earth*, *122*(5), 3574-3584, doi:10.1002/2017jb014059.

Liu, J., Hu, Q., Bi, W., Yang, L., Xiao, Y., Chow, P., et al. (2019), Altered chemistry of oxygen and iron under deep Earth conditions, *Nature Communications*, *10*(1), 153, doi:10.1038/s41467-018-08071-3.

Liu, J., Lin, J. F., Mao, Z., and Prakapenka, V. B. (2014), Thermal equation of state and spin transition of magnesiosiderite at high pressure and temperature, *American Mineralogist*, *99*(1), 84-93, doi:10.2138/am.2014.4553.

Lv, M., Liu, J., Zhu, F., Li, J., Zhang, D., Xiao, Y., et al. (2020), Spin transitions and compressibility of ε-$Fe_7N_3$ and γ′-$Fe_4N$: Implications for iron alloys in terrestrial planet cores, *Journal of Geophysical Research: Solid Earth*, *125*(11), B020660, doi:10.1029/2020jb020660.

Mao, H.-k., and Mao, W. L. (2020), Key problems of the four-dimensional Earth system, *Matter and Radiation at Extremes*, *5*(3), 038102, doi:10.1063/1.5139023.

Mao, H. K., Xu, J., and Bell, P. M. (1986), Calibration of the ruby pressure gauge to 800 kbar under quasi-hydrostatic conditions, *Journal of Geophysical Research: Solid Earth*, *91*(B5), 4673-4676, doi:10.1029/JB091iB05p04673.

Mao, Z., Lin, J. F., Yang, J., Wu, J., Watson, H. C., Xiao, Y., et al. (2014), Spin and valence states of iron in Al-bearing silicate glass at high pressures studied by synchrotron Mossbauer and X-ray emission spectroscopy, *American Mineralogist*, *99*(2-3), 415-423, doi:10.2138/am.2014.4490.

Margot, J.-L., Hauck II, S. A., Mazarico, E., Padovan, S., and Peale, S. J. (2018), Mercury's Internal Structure, in *Mercury: The View after MESSENGER*, edited by SC, S., LR, N. and BJ, A., pp. 85-113, Cambridge University Press, Cambridge

Marty, B. (2012), The origins and concentrations of water, carbon, nitrogen and noble gases on Earth, *Earth and Planetary Science Letters*, *313-314*, 56-66, doi:10.1016/j.epsl.2011.10.040.

Minobe, S., Nakajima, Y., Hirose, K., and Ohishi, Y. (2015), Stability and compressibility of a new iron-nitride β-$Fe_7N_3$ to core pressures, *Geophysical Research Letters*, *42*(13), 5206-5211, doi:10.1002/2015gl064496.

Monza, A., Meffre, A., Baudelet, F., Rueff, J. P., d'Astuto, M., Munsch, P., et al. (2011), Iron under pressure: "Kohn tweezers" and remnant magnetism, *Physical Review Letters*, *106*(24), 247201, doi:10.1103/PhysRevLett.106.247201.

Niellsen, H. P., and Burhwald, V. F. (1981), Roaldite, a new nitride in iron meteorites, paper presented at Proceedings Lunar and Planet Science Conference.

Niewa, R., Rau, D., Wosylus, A., Meier, K., Wessel, M., Hanfland, M., et al. (2009), High-pressure high-temperature phase transition of γ′-Fe4N, *Journal of Alloys and Compounds*, *480*(1), 76-80, doi:10.1016/j.jallcom.2008.09.178.

Ono, S. (2015), Relationship between structural variation and spin transition of iron under high pressures and high temperatures, *Solid State Communications*, *203*, 1-4, doi:10.1016/j.ssc.2014.11.010.

Panda, R. N., and Gajbhiye, N. S. (1997), Magnetic properties of single domain ε-$Fe_3N$ synthesized by borohydride reduction route, *Journal of Applied Physics*, *81*(1), 335-339, doi:10.1063/1.364115.

Popov, Z. I., Litasov, K. D., Gavryushkin, P. N., Ovchinnikov, S. G., and Fedorov, A. S. (2015), Theoretical study of γ′-$Fe_4N$ and ε-$Fe_xN$ iron nitrides at pressures up to 500 GPa, *JETP Letters*, *101*(6), 371-375, doi:10.1134/s0021364015060090.

Rohrbach, A., Ballhaus, C., Golla-Schindler, U., Ulmer, P., Kamenetsky, V. S., and Kuzmin, D. V. (2007), Metal saturation in the upper mantle, *Nature*, *449*(7161), 456-458, doi:10.1038/nature06183.

Rubin, A. E., and Ma, C. (2017), Meteoritic minerals and their origins, *Geochemistry*, *77*(3), 325-385, doi:10.1016/j.chemer.2017.01.005.

Schwarz, U., Wosylus, A., Wessel, M., Dronskowski, R., Hanfland, M., Rau, D., et al. (2009), High-pressure–high-temperature behavior of ζ-$Fe_2N$ and phase transition to ϵ-$Fe_3N_{1.5}$, *European Journal of Inorganic Chemistry*, *2009*(12), 1634-1639, doi:10.1002/ejic.200801222.

Sifkovits, M., Smolinski, H., Hellwig, S., and Weber, W. (1999), Interplay of chemical bonding and magnetism in $Fe_4N$, $Fe_3N$ and ζ-$Fe_2N$, *Journal of Magnetism and Magnetic Materials*, *204*(3), 191-198, doi:10.1016/s0304-8853(99)00296-6.

Slater, J. C. (1964), Atomic radii in crystals, *The Journal of Chemical Physics*, *41*(10), 3199-3204, doi:10.1063/1.1725697.

Smith, D. E., Zuber, M. T., Phillips, R. J., Solomon, S. C., Hauck, S. A., Lemoine, F. G., et al. (2012), Gravity field and internal structure of Mercury from MESSENGER, *Science*, *336*(6078), 214-217.

Stähler, S. C., Khan, A., Banerdt, W. B., Lognonné, P., Giardini, D., Ceylan, S., et al. (2021), Seismic detection of the martian core, *Science*, *373*(6553), 443-448, doi:10.1126/science.abi7730.

Su, X., Zhao, C., Xu, L., Lv, C., Song, X., Ishii, T., et al. (2021), Spectroscopic evidence for the $Fe^{3+}$ spin transition in iron-bearing δ-AlOOH at high pressure, *American Mineralogist*, *106*(11), 1709-1716, doi:doi:10.2138/am-2021-7541.

Sugiura, N. (1998), Ion probe measurements of carbon and nitrogen in iron meteorites, *Meteoritics & Planetary Science*, *33*(3), 393-409, doi:10.1111/j.1945-5100.1998.tb01645.x.

Tsuchiya, T., Wentzcovitch, R. M., da Silva, C. R., and de Gironcoli, S. (2006), Spin transition in magnesiowustite in earth's lower mantle, *Physical Review Letters*, *96*(19), 198501, doi:10.1103/PhysRevLett.96.198501.

Widenmeyer, M., Hansen, T. C., Meissner, E., and Niewa, R. (2014), Formation and decomposition of iron nitrides observed by in situ powder neutron diffraction and thermal analysis, *Zeitschrift fur Anorganische und Allgemeine Chemie*, *640*(7), 1265-1274, doi:10.1002/zaac.201300676.

Yoshioka, T., Wiedenbeck, M., Shcheka, S., and Keppler, H. (2018), Nitrogen solubility in the deep mantle and the origin of Earth's primordial nitrogen budget, *Earth and Planetary Science Letters*, *488*, 134-143, doi:10.1016/j.epsl.2018.02.021.

Zhao, C., Xu, L., Gui, W., and Liu, J. (2020), Phase stability and vibrational properties of iron-bearing carbonates at high pressure, *Minerals*, *10*(12), 1142, doi:10.3390/min10121142.

Zhuang, Y., Su, X., Salke, N. P., Cui, Z., Hu, Q., Zhang, D., et al. (2021), The effect of nitrogen on the compressibility and conductivity of iron at high pressure, *Geoscience Frontiers*, *12*(2), 983-989, doi:10.1016/j.gsf.2020.04.012.

This is the peer-reviewed, final accepted version for American Mineralogist, published by the Mineralogical Society of America.
The published version is subject to change. Cite as Authors (Year) Title. American Mineralogist, in press.
DOI: https://doi.org/10.2138/am-2022-8434. http://www.minsocam.org/

## Figure Captions

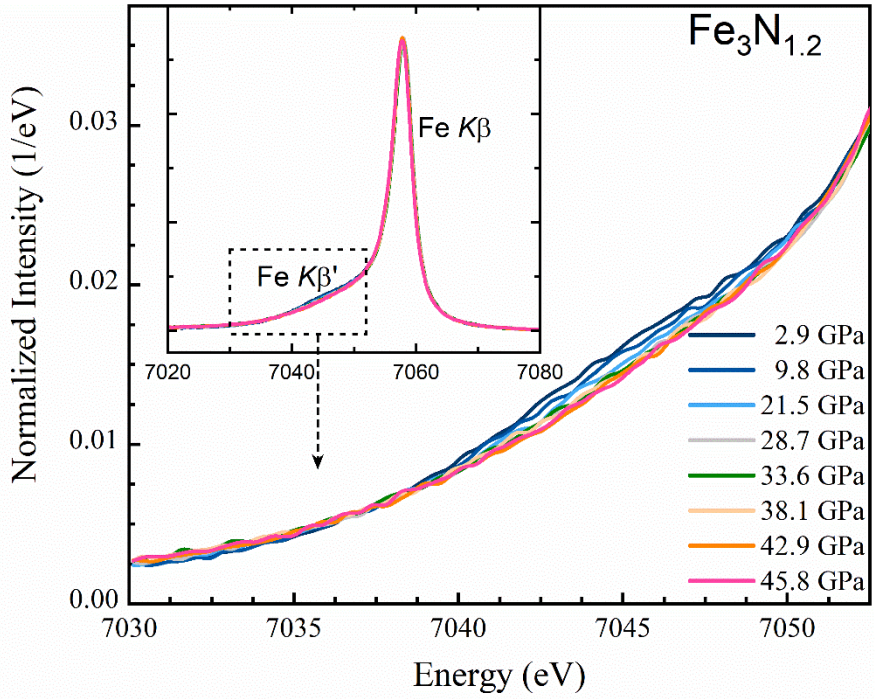


**Figure 1.** High-pressure XES spectra of $Fe_3N_{1.2}$ up to 45.8 GPa at 300 K. The XES spectra were normalized to unity in their integrated intensity. The insert is the full view of the Fe-$K_\beta$ fluorescence spectra from 7020 to 7080 eV, with the main peak aligned to 7058 eV. The reduction of the satellite peak with increasing pressure indicates the high-spin to low-spin transition of $Fe_3N_{1.2}$ under compression.

This is the peer-reviewed, final accepted version for American Mineralogist, published by the Mineralogical Society of America.
The published version is subject to change. Cite as Authors (Year) Title. American Mineralogist, in press.
DOI: https://doi.org/10.2138/am-2022-8434. http://www.minsocam.org/

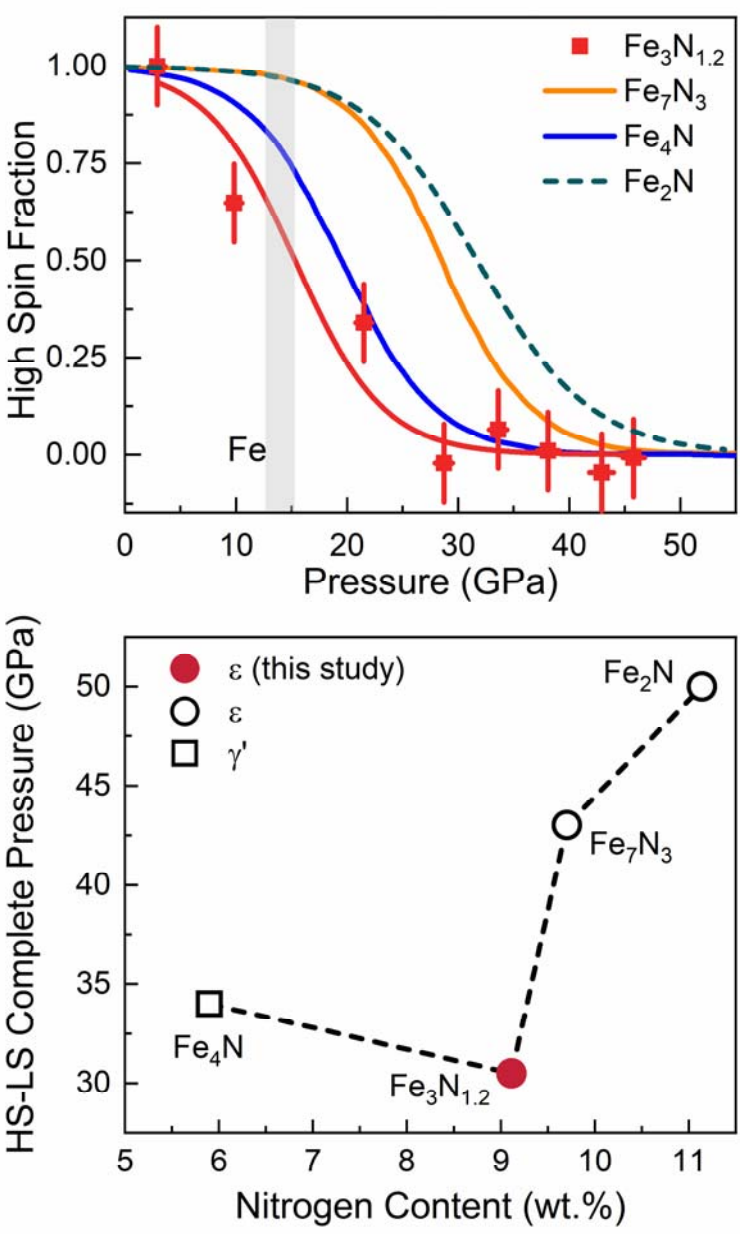


**Figure 2.** The complete pressure of spin transition in iron nitrides as a function of nitrogen content. The upper panel shows the high-spin fraction of Fe in iron nitrides as a function of pressure. The red squares show the high-spin fraction of hexagonal $Fe_3N_{1.2}$ derived from the XES measurements in this study. The spectrum at 2.9 GPa is adopted as the high spin reference spectrum while the average of nearly-unchanged spectra at 35−50 GPa is used as

437 the low spin reference spectrum. The red curve is the Boltzmann function fitting to the XES
438 data of $Fe_3N_{1.2}$. The solid yellow and blue curves represent the high-spin fraction for
439 hexagonal $Fe_7N_3$ and $Fe_4N$, respectively, derived from the XES experiments by *Lv et al.*
440 [2020]. The dashed olive curve is the iron spin transition of hexagonal $Fe_2N$ based on the
441 crystal axis ratio as a function of pressure [*Zhuang et al.*, 2021]. The volume jump of $Fe_2N$ at
442 10-20 GPa in *Zhuang et al.* [2021] may correspond to an isostructural phase transition such
443 as the FM-PM transition rather than the HS-LS transition. The grey zone indicates the spin
444 transition pressure (magnetic collapse) of pure Fe, which is accompanied simultaneously by
445 iron's bcc to hcp transition at 300 K [*Monza et al.*, 2011]. The lower panel shows the spin
446 transition complete pressure as a function of nitrogen content. Circle symbols represent
447 hcp-Fe-N phases, and the open square stands for fcc $Fe_4N$. The dashed lines are drawn to
448 guide the eye.

This is the peer-reviewed, final accepted version for American Mineralogist, published by the Mineralogical Society of America.
The published version is subject to change. Cite as Authors (Year) Title. American Mineralogist, in press.
DOI: https://doi.org/10.2138/am-2022-8434. http://www.minsocam.org/

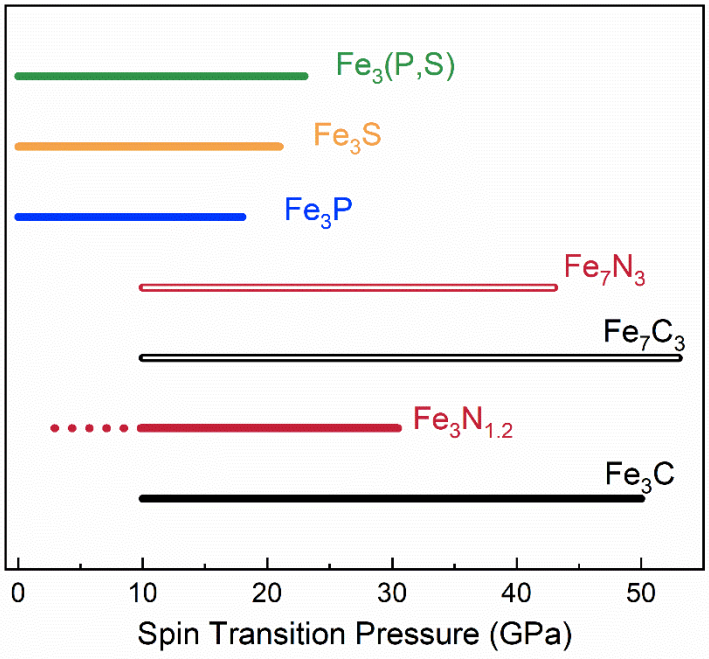


**Figure 3.** Spin transition pressure of iron-rich nitrides, carbides, phosphides, and sulfides. Each line shows the pressure range of the iron spin transition for a given phase. The left and right ends of the lines denote the onset and completion pressures of the HS-LS transition, respectively. The dotted line of $Fe_3N_{1.2}$ indicates the uncertainty of the onset pressure of the HS-LS transition. Literature data for $Fe_3P$ and $Fe_3(P,S)$ are from XES experiments in *Gu et al.* [2016], $Fe_3S$ from SMS experiments in *Lin et al.* [2004a], $Fe_3C$ and $Fe_7C_3$ from XES experiments in *Chen et al.* [2018], and $Fe_7N_3$ from XES experiments in *Lv et al.* [2020].